COMPUTATIONAL FLUID DYNAMICS MODELING AND VALIDATION OF SWIRLING FLOW IN A PIPE WITH CLASSIC TWISTED TAPE

Minseop Song, So Hyun Park, and Eung Soo Kim*
Seoul National University, South Korea
kes7741@snu.ac.kr
ssrmin@snu.ac.kr; bibirom@snu.ac.kr

ABSTRACT

The twisted tape is a passive equipment enhancing the heat transfer capability of a heat exchanger. This technique was adopted in various industries including nuclear engineering to improve economic efficiency. Previous researchers used computational fluid dynamics (CFD) method to predict the performance of heat exchanger with twisted tape. Existing literatures insisted that simulation result with k-omega model most corresponds with the experimental data on friction factor, Nusselt number. However, fluid behavior in twisted tape was not validated due to the lack of experimental data. As the optical access to the inner space of a pipe with a twisted tape was limited, the detailed flow field data were not obtainable so far. The fluid behavior is important for optimization of shape of twisted tape in terms of size, pitch and distance between tapes.

In this study, 2-Dimensional fluid velocity data was measured using particle image velocimetry (PIV) in wide Reynolds number range of 1370 ~ 9591. The test section was made by 3D printing technique of stereolithography. It enabled the production of transparent test section for optical access. A distortion due to difference of refractive indices of fluid and test section was diminished by matching the refractive index. A noble working fluid, which is mixture of herb oil and mineral oil, was used.

The experimental data was compared with simulation result of various turbulent models. The PIV data showed characteristic two-peak motion in axial direction. The CFD simulation used standard k-epsilon and standard k-omega turbulence model. The geometry of fluid region in CFD was perfectly depicted as real flow path. The result showed that k-e turbulence model is proper to use for prediction of flow behavior in flow around twisted tape.

KEYWORDS
Computational Fluid Dynamics, Twisted Tape, Particle Image Velocimetry, Swirling Flow, Matching Index of Refraction, 3D Printing

1. INTRODUCTION

Twisted tape is a one of the passive equipment designed to enhance the performance of heat exchanger. Previous researches proved that the increase of the turbulent intensity in flow and its swirl motion increase the heat transfer efficiency [1]. In the nuclear engineering fields, twisted tape is selected as heat-transfer-enhancement device for the divertor in ITER. Twisted tape is inserted in the vertical target, which

---

* Assistant Professor, Department of Nuclear Engineering, Seoul National University, South Korea

is the most important device of divertor, increasing the limit of critical heat flux [2]. Therefore, accurate study on the thermohydraulic performance of flow around twisted tape is important topic. Besides, analyzing the flow behavior of swirling flow induced by twisted tape is of importance in finding out heat transfer enhancement mechanism.

Previous researches used the computational fluid dynamics modeling, which is distributed parameter analysis method to calculate the flow and heat transfer performance of swirling flow around twisted tape [3, 4, 5]. Previous research reported that simulation result with k-omega model most corresponds with the experimental data on friction factor and Nusselt number. However, fluid behavior in twisted tape was not validated due to the lack of experimental data. As the optical access to the inner space of a pipe with a twisted tape was limited, the detailed flow field data were not obtainable so far.

The aim of this research project, therefore, has been to find out the most proper turbulence model in analyzing the flow behaviors around twisted tape. To find out a proper turbulence model for simulation of swirling flow, the results from different turbulence models were compared with measurement data obtained by Particle Image Velocimetry.

2. EXPERIMENTAL SETUP

2.1. Test Section Geometry

Test section was composed of cylindrical tube and classical twisted tape as illustrated in the Fig. 1. As width of twisted tape was equal to the diameter of pipe, no gap between the tape and the pipe exist. Once fluid entered the pipe, therefore, it did not mix with fluid of the opposite side. The characteristic parameters of twisted tape are listed in the Table 1. Twisted tape rotated 12 times, and total length over diameter (L/D) was 36.

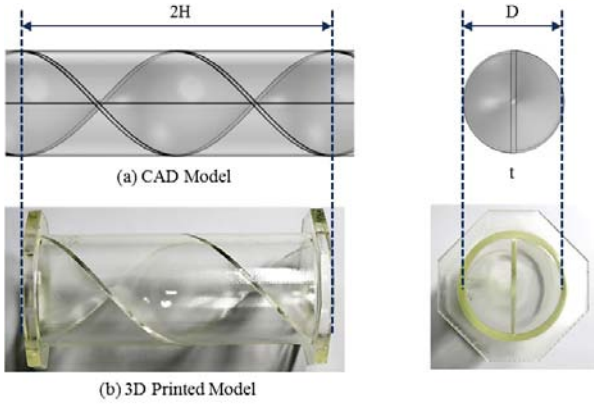

Figure 1. Geometry of Test Section and 3D-Printed Test Section.

Table I. Geometry Parameters of Twisted Tape

Parameter	Value
Twist Pitch (180°), H	57 mm
Pipe Diameter, D	38mm
Tape Thickness, t	2mm
Twist ratio, y	1.5

2.2. Test Section Fabrication

A test section was produced by using 3D printer. The 3D printer sintering model materials using laser is called Stereolithography 3D printer. The strong point of 3D printer is to make any complex model accurately. Therefore, 3D printer made it possible to make geometry of helically twisted tape in pipe. Although many type of 3D printers developed, SLA type 3D printer is most possible option to make transparent model with high quality. Song et al showed that transparent test section made by SLA type 3D printer have possibilities to be used in flow visualization experiments [6]. The model name of 3D printer is RM-6000 2 of CMET. The basic material of model was TSR-829, epoxy based. The minimum layer thickness of layer was 50um and the layer thickness of test section made was 100um. Flexural modulus of printed model is large enough as 1,840MPa, and it is higher than that of acryl; 496 ~ 1172MPa [6]. The refractive index of transparent model is 1.5105 at the wavelength of 532nm [6].

SLA type 3D printers usually build the model parallel to the ground. However, it was observed that the transparent model made parallel to the ground did not display its interior area clearly. Butscher et al experienced same phenomenon [7]. They reported transparent models build at an angle of 45 degrees showed better quality in particle image. Fig. 2 shows particle images of each case. First image was captured at the test section layered parallel to the ground and the second image was captured after changing the angle of layer. While particles in image (b) keep the circle shape, the particles in image (a) are stretched vertically. This result may be explained by the diffraction. When the light pass through gap of layer, it disperse in perpendicular direction. The vertical lines of particles in (a) support this assumption. As elongated particle in image could broaden the correlation peak of cross correlation, it should be avoided. Broadened correlation peak lower the accuracy of the algorithm by giving wrong displacement vectors. Thus, the test section for flow visualization was built by tilting in 45 degrees.

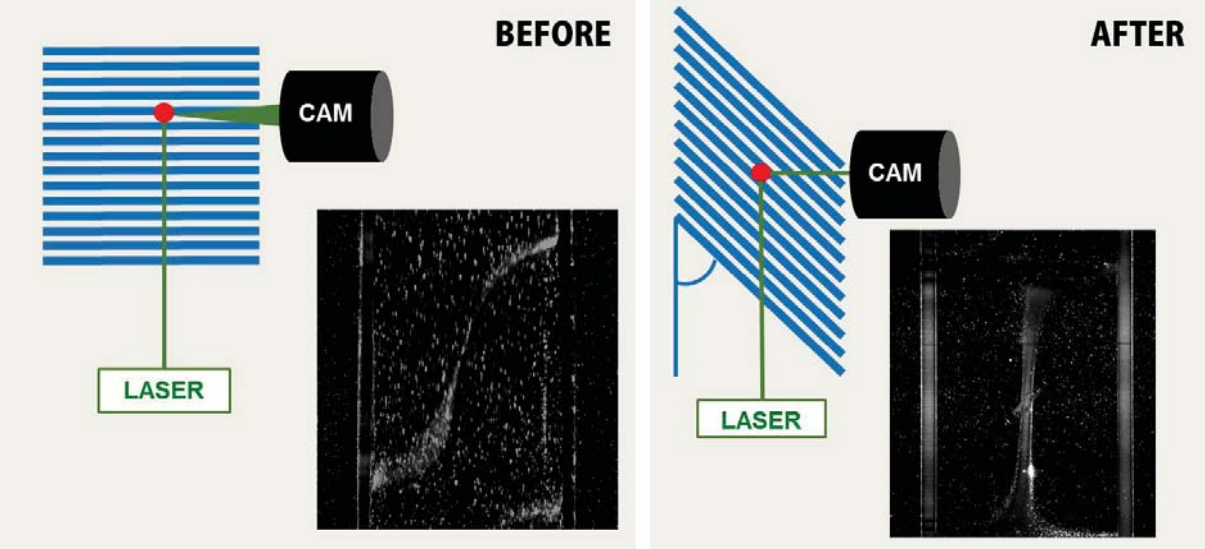

Figure 2. Different Particle Images according to the Angle of the Layer.

2.3. Working Fluid

The mixture of anise oil and mineral oil was used as working fluid [6]. This mixture had light color, water-like density. The refractive index of mixture was adjustable, and the range of refractive index was from 1.45 to 1.55. The refractive index of 3D printed model determined the mixture ratio of working

fluid. The ratio of anise oil was 0.598 and that of mineral oil was 0.402. The refractive index of mixture was measured to be 1.514 after mixing. The relative difference with 1.5105 was 0.2%. Thus, density and viscosity of mixture was calculated from the actual ratio. Equation (1), (2) and (3) are the correlation used to calculate the refractive index, density and viscosity of mixture [6]. V_A represents the volume ratio of anise oil.

$$RI_{Mixture} = V_A \cdot RI_{Anise} + (1 - V_A) \cdot RI_{Mineral\ Oil} \tag{1}$$

$$\rho_{Mixture} = V_A \cdot \rho_{Anise} + (1 - V_A) \cdot \rho_{Mineral\ Oil} \tag{2}$$

$$ln\mu_{Mixture} = x_A \cdot ln\mu_{Anise} + x_B \cdot ln\mu_{Mineral\ oil}\, x, \quad x_A = \frac{V_A}{V_A + 0.28 \cdot V_B}, \quad x_B = 1 - x_A \tag{3}$$

The density of mixture was calculated as 915kg/m^3. The density smaller than water guarantee the use of existing tracer particles like silver-coated hollow glass (density: 1080 kg/m^3) and polyamide (density: 1030 kg/m^3). In this study, silver-coated hollow glass was used in the average diameter of 15um.

2.4. Refractive Index Matching

The refractive indices of 3D printer and working fluid were matched to remove optical distortion of light. When the refractive indices of two material are matched, the refraction of light is reduced. Therefore, the position of particles in the image was maintained as its original one. The mixed oil had circulated in the loop for 2 hours for mixing. After that, the mixture filled the space between 3D printed model and square viewing box of glass. Thus, lights reflected from particles doesn`t experience the refraction until it reaches the viewing box.

Fig. 3 shows the comparison result of the clarity of the image of test section. The dot image was placed behind the test section for the test. As the light reflected in the image was in the range of visible light, actual refraction is different from the refraction of green light. However, this image gave enough information about the visibility of test section. Evidently, background image was shown clear in refractive index matched case. Although the refractive index is matched, dot image was blurred at the line of the twisted tape. As it can harm the accuracy of cross correlation, this part was masked in image processing process.

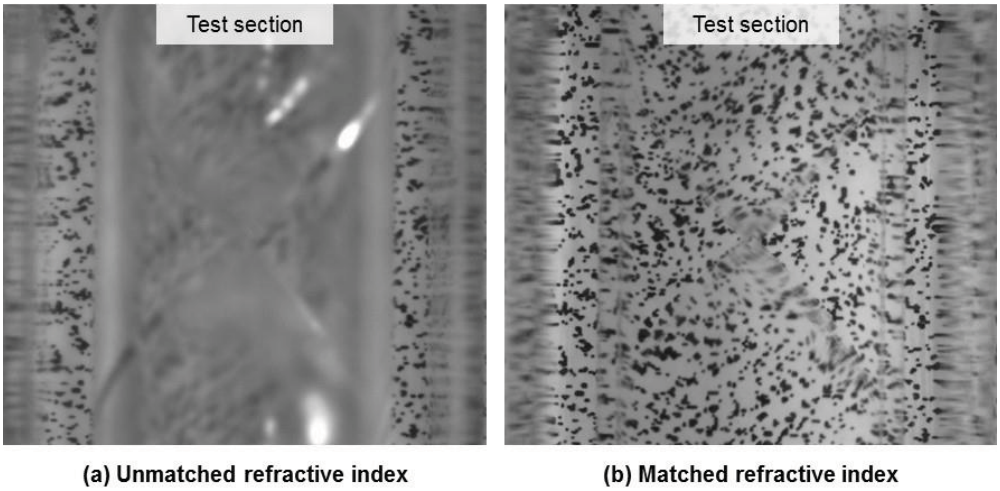

Figure 3. Refraction Index Matching Test Result.

2.5. Circulation Loop

The form of loop used for experiment was closed circulation loop. All parts were consist of chemically resistance materials such as stainless steel in consideration of reaction with the working fluid. Acryl was excluded because it react with anise oil. Fig. 4 shows the schematic diagram of circulation loop. Oil mixture flowed downward from the tank and was pressurized by the centrifugal pump. The bulk velocity of working fluid is measured using Coriolis flow meter, which have accuracy of 0.1%. It was designed to for working fluid to flow in downward to take images at the bottom.

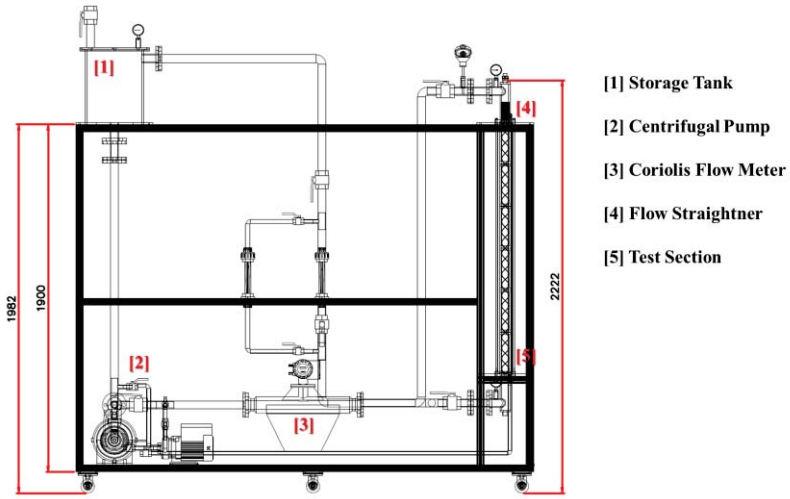

Figure 4. Experimental Circulation Loop

3. Particle Image Velocimetry Setup

3.1. Camera and Laser

Particle image velocimetry system contains CCD camera and laser generator to capture the particle image in the fluid. Double pulse Nd:Yag laser of wavelength at 532nm illuminate plane laser beam sheet to the test section with thickness of 1~2mm. The distance between laser and test section and focal lens were precisely adjusted to place the focal point of laser to the test section. The reflected green laser light was captured by PCO 1600 CCD camera with resolution of 1600x1200 in 14 bit. Particle image is stored to the 172 pairs owing to the limit of storage of the 2G RAM. Camera and laser generator was controlled by synchronizer.

3.2. Measurement Location

The particle image pairs were captured at the 228mm height from the bottom of the test section. The area of measurement plane is 86.68mm x 65.01mm. 1pixel represent 0.00541mm in real scale. Laser sheet lighted three plane with different z height. Fig. 5 shows the shape of each measurement plane.

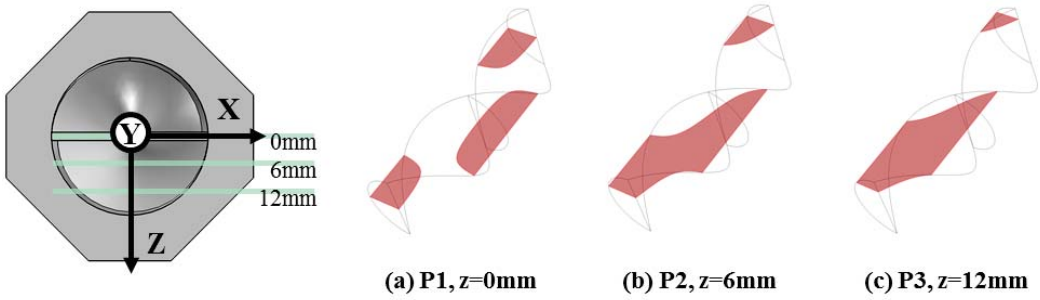

Figure 5. Measurement Plane View

3.3. Particle Image Velocimetry Algorithm

In the particle image velocimetry program, PIVview 2C, the particle image was divided into small area, called interrogation area. The size of interrogation area was set to 32x32 pixels, and the step size was 16x13. No dependency on the size of the interrogation area and the ratio of long side to short side of interrogation area was found. During correlating the interrogation area, nyquist frequency filtering was adjusted to remove effect of noise. Multi-grid interrogation method was applied to find vector more precisely from larger interrogation area. The initial interrogation size was set to 128x128. Finally, sub-pixel peak searching was performed by 3-point Gaussian fit method.

3.4. Flow Condition

Inlet flow was controlled by pump which communicates with Coriolis flow meter. The Coriolis flowmeter measured the flow rate in mass unit (kg/min). Thus, flow rate was measured as unit of mass flow rate. The mass flow rate ranges from 5 to 35 for one channel. Reynolds number and average velocity, time distance was listed in the TableII. The time distance was set for z-directional displacement of particle not to exceed thickness of laser sheet of 1mm.

Table Ⅱ. Flow Condition of Experiment

Mass Flow Rate (kg/min)	Re	Average Velocity (m/s)	Time Distance (us)
5	1370	0.188	1314
15	4110	0.563	438
25	6851	0.938	266
35	9591	1.313	190

4. CFD Modeling

Computational fluid dynamics simulation was performed using COMSOL multiphysics code V5.0. COMSOL multiphysics code is a commercial code that have ability to simulate various physics simultaneously. In this research, only single-phase flow physics was used.

Same geometry of the test section was imported from the CAD files designed for the 3D printing. As two flow paths in pipe with twisted tape is identical, only one side of the flow path was used. The properties like density and viscosity of working fluid, mixture of anise oil and mineral oil, were imputed from the calculated values above.

Two turbulence model, k-e and k-w, were used to simulate the turbulence flow. These two turbulence models are kinds of Reynolds averaged Navier-stokes equations that use turbulent kinetic energy, turbulent dissipation rate and specific dissipation rate to approximate the turbulent eddy viscosity. Equation (4) ~ (12) represent all the equations used in simulation. The coefficient used for the turbulence model was not changed from the basic settings.

$$\rho\nabla\cdot\boldsymbol{u}=0 \tag{4}$$

$$\rho(\boldsymbol{\nabla}\cdot\boldsymbol{u})\boldsymbol{u}=\nabla\cdot[-p\mathbf{I}+(\mu+\mu_T)\left(\nabla\boldsymbol{u}+(\nabla\boldsymbol{u})^T-\frac{2}{3}\rho k\mathbf{I}\right]+\mathbf{F} \tag{5}$$

For k-e turbulence models,

$$\rho(\boldsymbol{u}\cdot\boldsymbol{\nabla})k=\nabla\cdot\left[\left(\mu+\frac{\mu_T}{\sigma_k}\right)\nabla k\right]+P_k-\rho\varepsilon \tag{6}$$

$$\rho(\boldsymbol{u}\cdot\boldsymbol{\nabla})\varepsilon=\nabla\cdot\left[\left(\mu+\frac{\mu_T}{\sigma_\varepsilon}\right)\nabla\varepsilon\right]+C_{\varepsilon1}\frac{\varepsilon}{k}P_k-C_2\rho\frac{\varepsilon^2}{k} \tag{7}$$

$$\mu_T=\rho C_\mu\frac{k^2}{\varepsilon} \tag{8}$$

$$P_k=\mu_T[\nabla\boldsymbol{u}:(\nabla\boldsymbol{u}+(\nabla\boldsymbol{u})^T)] \tag{9}$$

For k-w turbulence models,

$$\rho(\boldsymbol{u}\cdot\boldsymbol{\nabla})k=\nabla\cdot[(\mu+\mu_T\sigma_T^*)\nabla k]+P_k-\beta_0^*\rho\omega k \tag{10}$$

$$\rho(\boldsymbol{u}\cdot\boldsymbol{\nabla})\omega=\nabla\cdot[(\mu+\mu_T\sigma_\omega)\nabla\omega]+\alpha\frac{\omega}{k}P_k-\rho\beta_0\omega^2 \tag{11}$$

$$\mu_T=\rho\frac{\omega}{k} \tag{12}$$

$$P_k=\mu_T[\nabla\boldsymbol{u}:(\nabla\boldsymbol{u}+(\nabla\boldsymbol{u})^T)]-\frac{2}{3}\rho k\boldsymbol{\nabla}\cdot\boldsymbol{u} \tag{13}$$

The inlet boundary condition was set as normal inflow velocity. The velocity values are the same as bulk velocity used in PIV experiments. Constant pressure boundary condition was applied and the pressure at the plane of outlet was 13000Pa. Wall functions simulated the boundary layer. The geometry was meshed with combinations of tetrahedral, prism, triangular and quadrilateral elements. Total number of elements was 420145 with the average volume of 6.69E-4m^3.

5. RESULT AND DISCUSSION

5.1. Particle Image Analysis

Fig. 6 illustrate raw particle image captured by CCD camera at plane 1. Twisted tape reflected the laser at the center of the pipe and lower part. As lower part reflected much of light, image of this part was not proper. As mentioned earlier, particles under the twisted tape blurred. Reflected light was also observed at the bottom where the twisted tape was parallel to the laser sheet. In this region, the particles were scarcely distinguishable. Thus, these two regions were masked not to be included in the vector calculation. Except for those regions, particle images of other parts were clearly acquired. The position of origin was set to the place where the line of tapes cross.

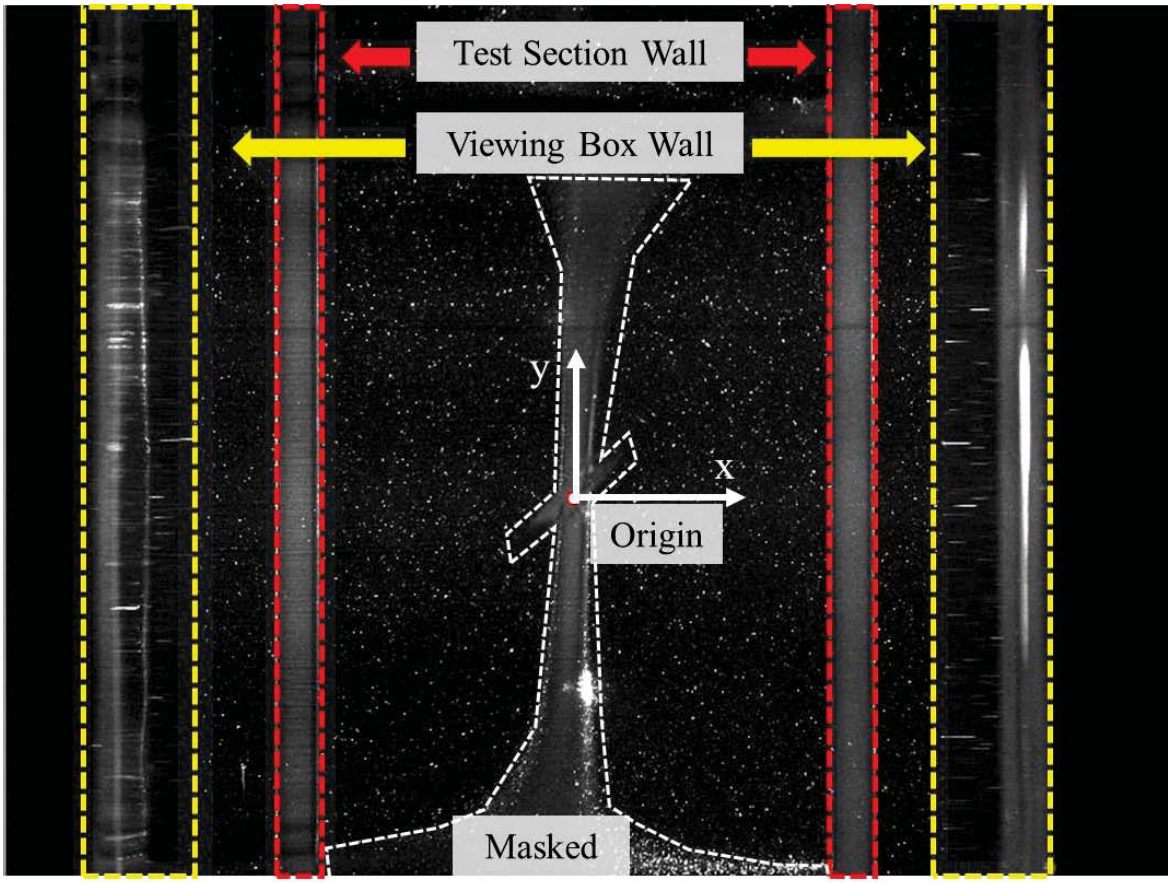

Figure 6. Particle Image at Plane 1

5.2. Mean Convergence Test

Mean convergence test was performed to assure whether the number of image pair was secured. Fig. 7 shows the mean convergence plot of u and v component. The point of measurement was located at -9.125, 11.33 in the coordinate of the PIV image. This point was selected as it is far from the wall and tape. Mean convergence plot shows that the mean converged around 100th cases. For the u-component convergence speed was little slower than the v-component. This result have two possible causes. At first, it could mean that the turbulence intensity of u component, which is proportional to the wall, is stronger than that of v

component. The other one is the limitation of PIV algorithm. The size of interrogation area was selected based on the bulk velocity in direction of v. In all cases, mean of v component is larger than the u component. Therefore, small displacement in x-axis compared to large displacement in y-axis could cause an inaccurate peak detection in x-axis. This fact lower the confidence of u component.

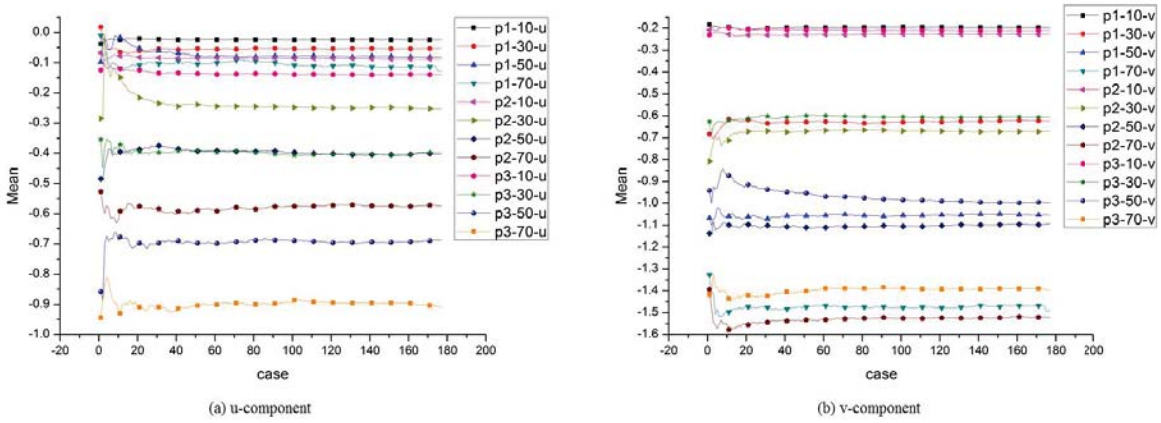

Figure 7. Mean convergence Test Result of u and v component

Based on the 177 pairs of particle images, two-dimensional velocity fields and contour results were obtained. Fig. 8 represent vector field and contour images at the Reynolds number of 9591. Different masks were applied to images according to the shape of reflection light of the laser sheet. It can be observed that mask rotate as the z level of plane increases along with the location of twisted tape. The entire mean velocity vector identically headed left low part. Another feature in this figure was distribution of velocity magnitude value. In the plane 1 and plane 3, velocity contour shows typical one peak profile as color, the center of the space peaking highest velocity. However, in the plane 2, upper side of velocity field shows two-peak like gradient distribution. This feature was observed in any Reynolds number condition identically

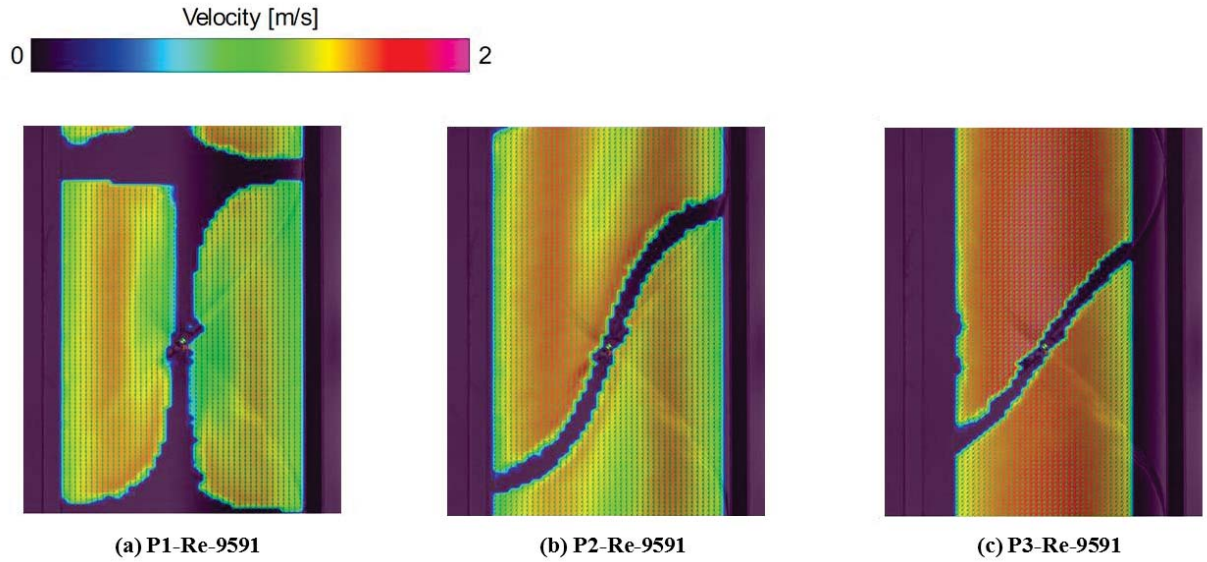

Figure 8. Velocity Magnitude Contour Images at Re=9591

5.2. Comparison between PIV and CFD Result

Velocity data from PIV and CFD simulation result using the k-e and k-w turbulence model were compared. Measurement points were located along lines of y=0 from the origin to the y-direction. The direction of this line is identical to the radial direction in cylindrical system, thus it means the velocity distribution along the radius. The x-axis in plane 2, 3 doesn`t have special meaning in position but should be observed for comparison.

Fig. 9 represents graphs that compare the velocity magnitude data from PIV and CFD in k-e, k-w. Total 12 case of graphs were produced. The most common feature of graphs was discrepancy of wall velocity between PIV and CFD results. It was caused by the limitation of analytical ability of PIV near the wall. As the interrogation area near the wall contains region of zero signal, it cannot interpret velocity accurately. Additionally, large velocity gradient near the wall needs more spatially resolved interrogation area. Even though the interrogation area can be reduced as want, if it doesn`t contain enough number of particle images, it would not draw a precise result. On the other hand, the CFD code used wall function, it could be more similar to true value, but it needs still validation. Thus, comparison of velocity near the pipe wall and twisted tape is meaningless yet. To obtain velocity data near the wall, it is planned to introduce laser doppler anemometry. LDA can measure the velocity at a point with very high temporal and spatial resolution. With this analysis of the error source near the wall region, it is concluded that the comparison of data from PIV and CFD is meaningful only in the middle of flow path.

Some features were observed from the graphs. First is consistency of shape of the profiles. In plane 1, the velocity magnitude of k-e, k-w model result show similar one peak shape. However, the line of PIV result show different shape. It have halfway at the center of the radius. As velocity increase, data from k-e model follow PIV data but profile of k-w model didn`t. This trend is more certain in the plane 2. Characteristic two-peak profile of PIV data appear up from the Re 1370. As Re increases, k-e and k-w profiles of model data follow the first peak near the twisted tape, but two-peak profile only is shown in the data from k-e model. Tendency of profile in plane 3 is different from plane 1 and 2. Profile of PIV data in high Re is more close to the k-w model. This result are likely to be related to position of the plane 3. In contrast to plane 1 and 2, plane 3 is closely packed with tape and wall. Thus, same with the explanation above, data from PIV is less accurate.

This observational study suggest that the calculation result from k-e model predict the swirl motion in twisted tape better than result from k-w model. Although two-equation turbulence model is not accurate for flow with streamline curvature, this result tells that k-e model have ability to predict true value in a certain degree. As the strengths of k-e model comparing to other turbulence model are its conciseness and fast convergence speed, calculating turbulence flow with swirling motion using k-e model would be efficient way.

What is interesting in this data is comparison of normalized velocity magnitude profile of different Re number. Graphs in Fig. 10 composed the normalized velocity profiles of different Reynolds numbers at each plane. The velocity magnitude data from PIV was divided by bulk velocity of each Reynolds number. The normalized velocity magnitude profiles, except for profile of Re 1370, is almost identical especially at the center. The difference of profile of Re 1370 can be explained in flow regime. It is suspected that flow at Re 1370 is in the different flow regime like laminar flow or transient flow. The identical profile of higher Re flow seems to be in the same turbulence regime. As the profile didn`t change with Reynolds number, it could be concluded that the velocity profile of twisted tape obtained from PIV can be used in predicting velocity profile of different Reynolds number. This result is will be only valid for non-decaying flow.

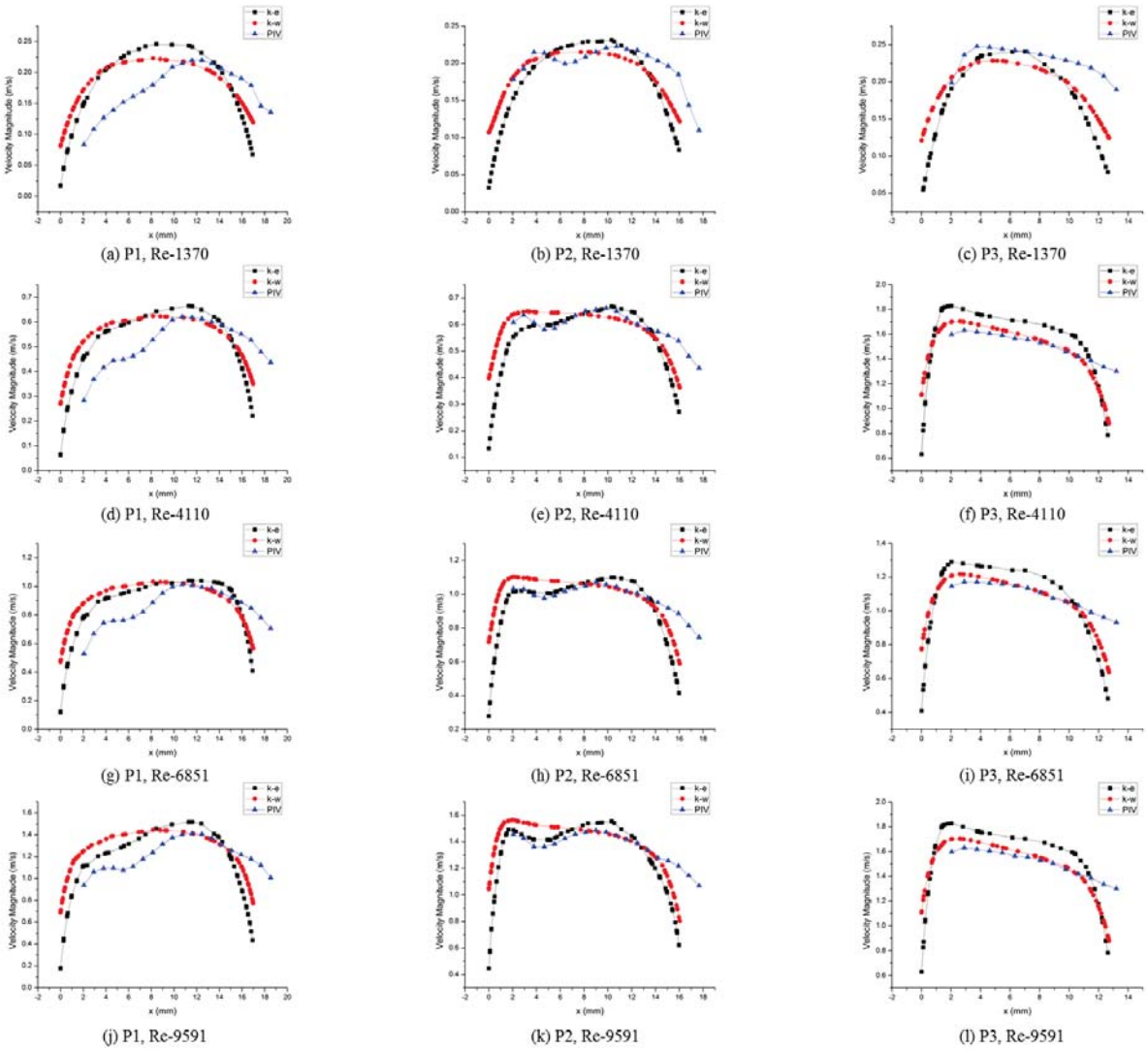

Figure 9. Velocity Magnitude of PIV and CFD

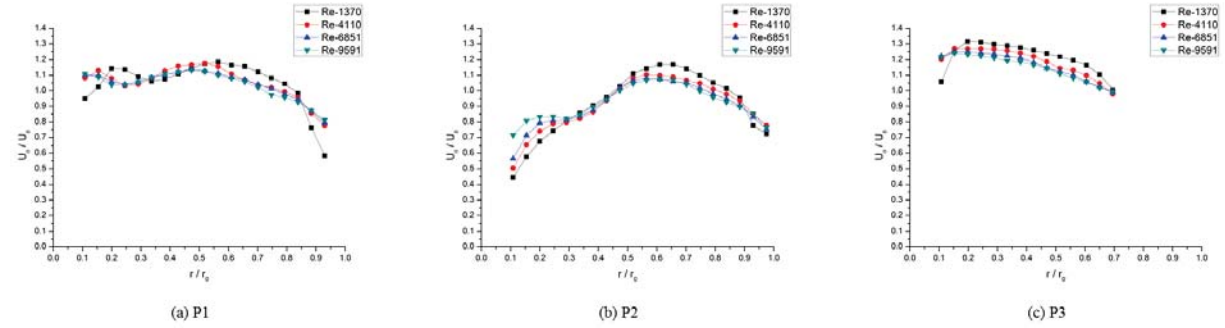

Figure 10. Normalized Velocity Magnitude by Bulk Velocity

6. CONCLUSIONS

For two type of turbulence model, k-e and k-w, CFD modeling for swirl flow in pipe with twisted tape has been performed and validated by the experiment data from PIV. To measure the velocity field in pipe with twisted tape, 3D printing and matching index of refraction technique was applied. These techniques successfully enabled to obtain clear image of particles for PIV analysis. From the images, velocity field data of 3 different plane and 4 kind of flow condition were made. The CFD modeling was performed also for the same condition with experiments. CFD modeling for k-e and k-w turbulence model were performed.

The PIV result was used to validate the CFD result from different turbulence models. The velocity field of PIV data near the wall and twisted tape didn`t accept to be accurate because of limitation PIV algorithm and its strong swirling flow motion. Thus, the measurement data for the middle of the space was used to validate CFD result. From the graphs, it was concluded that k-e turbulence model predict the swirl flow in pipe more accurately based on the degree of consistency of profiles. The k-e model shows the characteristic two-peak profile like PIV result. Although two-equation turbulence modeling was known inaccurate for swirling flow as stream curvature, k-e modeling displayed certain degree of accuracy. The normalized velocity magnitude profile also proved that velocity profile would not change largely for non-decaying swirl flow.

Further studies will be performed with combinations of LDA measurement. LDA study for test section with refractive index matched will give very accurate boundary layer data.

ACKNOWLEDGMENTS

This work was supported by the National R&D Program provided by the National Research Foundation of Korea (NRF) grant funded by MSIP (Ministry of Science ICT & Future Planning) [No. 0620-20140032]. This work was also supported by the Nuclear Safety Research Program through the Korea Radiation Safety Foundation (KORSAFe), granted financial resource from the Nuclear Safety and Security Commission (NSSC), Republic of Korea [No. 0620-20140049].

REFERENCES

1. S. R. Shabanian, M. Rahimi, M. Shahhosseini, and A. A. Alsairafi, “CFD and experimental studies on heat transfer enhancement in an air cooler equipped with different tube inserts”, *International Communications in Heat and Mass Transfer*, **38**, p. 383 (2010)
2. H. Nakaharai, S. Takami, T. Yokomine, S. Ebara, and A. Shimizu. “Numerical Study of Heat Transfer Characteristics in a Tube with Regularly Spaced Twisted Tape.” *Fusion Science and Technology 52*, **4**, pp. 855–59 (2007)
3. A. W. Date, “Prediction of fully-developed flow in a tube containing a twisted-tape”, *International Journal of Heat and Mass Transfer*, **17**, p.845 (1974)
4. J. P. Du Plessis, D. G. Kroger, “Friction factor prediction for fully developed laminar twisted-tape flow”, *International Journal of Heat and Mass Transfer*, **27**, p. 2095 (1984)
5. R. M. Manglik, A. E. Bergles, “Heat transfer and pressure drop correlations for twisted tape inserts in isothermal tubes: Part2-Transition and Turbulent Flows”, *J. Heat Transfer,* **115**, p. 890 (1993)
6. M. S. Song, H. Y. Choi, J. H. Seong, and E. S. Kim. “Matching-Index-of-Refraction of Transparent 3D Printing Models for Flow Visualization.” *Nuclear Engineering and Design*, **284**, pp. 185-191 (2015)
7. D. Butscher, C. Hutter, S. Kuhn, and P. R. von Rohr. “Particle Image Velocimetry in a Foam-like Porous Structure Using Refractive Index Matching: A Method to Characterize the Hydrodynamic Performance of Porous Structures.” *Experiments in Fluids 53*, **4**, pp. 1123–32 (2012)